

RESEARCH ARTICLE

Insights on the impact of mitochondrial organisation on bioenergetics in high-resolution computational models of cardiac cell architecture

Shouryadipta Ghosh^{1,2}, Kenneth Tran³, Lea M. D. Delbridge⁴, Anthony J. R. Hickey⁵, Eric Hanssen⁶, Edmund J. Crampin^{2,7}, Vijay Rajagopal^{1*}

1 Cell Structure and Mechanobiology Group, Dept. of Biomedical Engineering, Melbourne School of Engineering, University of Melbourne, Melbourne, Australia, **2** Systems Biology Laboratory, School of Mathematics and Statistics, and Melbourne School of Engineering, University of Melbourne, Melbourne, Australia, **3** Auckland Bioengineering Institute, University of Auckland, Auckland New Zealand, **4** Department of Physiology, University of Melbourne, Parkville, Australia, **5** School of Biological Sciences, University of Auckland, Auckland, New Zealand, **6** Advanced Microscopy Facility, Bio21 Molecular Science and Biotechnology Institute, The University of Melbourne, Melbourne, Australia, **7** ARC Centre of Excellence in Convergent Bio-Nano Science and Technology, University of Melbourne, Melbourne, Australia

* vijay.rajagopal@unimelb.edu.au



OPEN ACCESS

Citation: Ghosh S, Tran K, Delbridge LMD, Hickey AJR, Hanssen E, Crampin EJ, et al. (2018) Insights on the impact of mitochondrial organisation on bioenergetics in high-resolution computational models of cardiac cell architecture. *PLoS Comput Biol* 14(12): e1006640. <https://doi.org/10.1371/journal.pcbi.1006640>

Editor: Andrew D. McCulloch, University of California San Diego, UNITED STATES

Received: May 24, 2018

Accepted: November 13, 2018

Published: December 5, 2018

Copyright: © 2018 Ghosh et al. This is an open access article distributed under the terms of the [Creative Commons Attribution License](https://creativecommons.org/licenses/by/4.0/), which permits unrestricted use, distribution, and reproduction in any medium, provided the original author and source are credited.

Data Availability Statement: Codes to simulate the spatiotemporal dynamics of cardiac cell metabolites are freely available at: https://github.com/CellSMB/cardiac_bioenergetics. The high resolution spatial models associated with the finite element simulations can be found at the same URL. The raw serial block face electron microscopy data used to generate the models are available at <https://github.com/CellSMB/sbfsem-cardiac-cell-segmenter-v1/blob/master/Cell%20Segmenter%20v1/sbfsem-cardiac-cell-segmenter-master.zip>.

Abstract

Recent electron microscopy data have revealed that cardiac mitochondria are not arranged in crystalline columns but are organised with several mitochondria aggregated into columns of varying sizes spanning the cell cross-section. This raises the question—how does the mitochondrial arrangement affect the metabolite distributions within cardiomyocytes and what is its impact on force dynamics? Here, we address this question by employing finite element modeling of cardiac bioenergetics on computational meshes derived from electron microscope images. Our results indicate that heterogeneous mitochondrial distributions can lead to significant spatial variation across the cell in concentrations of inorganic phosphate, creatine (Cr) and creatine phosphate (PCr). However, our model predicts that sufficient activity of the creatine kinase (CK) system, coupled with rapid diffusion of Cr and PCr, maintains near uniform ATP and ADP ratios across the cell cross sections. This homogenous distribution of ATP and ADP should also evenly distribute force production and twitch duration with contraction. These results suggest that the PCr shuttle and associated enzymatic reactions act to maintain uniform force dynamics in the cell despite the heterogeneous mitochondrial organization. However, our model also predicts that under hypoxia activity of mitochondrial CK enzymes and diffusion of high-energy phosphate compounds may be insufficient to sustain uniform ATP/ADP distribution and hence force generation.

Funding: This research was in part conducted and funded by the Australian Research Council Centre of Excellence in Convergent Bio-Nano Science and Technology (project number CE140100036) and the Australian Research Council's Discovery Projects funding scheme (project DP170101358). The funders had no role in study design, data collection and analysis, decision to publish, or preparation of the manuscript.

Competing interests: The authors have declared that no competing interests exist.

Author summary

Mammalian cardiomyocytes contain a high volume of mitochondria, which maintains the continuous and bulk supply of ATP to sustain normal heart function. Previously, cardiac mitochondria were understood to be distributed in a regular, crystalline pattern, which facilitated a steady supply of ATP at different workloads. Using electron microscopy images of cell cross sections, we recently found that they are not regularly distributed inside cardiomyocytes. We created new spatially accurate computational models of cardiac cell bioenergetics and tested whether this heterogeneous distribution of mitochondria causes non-uniform energy supply and contractile force production in the cardiomyocyte. We found that ATP and ADP concentrations remain uniform throughout the cell because of the activity of creatine kinase (CK) enzymes that convert ATP produced in the mitochondria into creatine phosphate. Creatine phosphate rapidly diffuses to the myofibril region where it can be converted back to ATP for the contraction cycle in a timely manner. This mechanism is called the phosphocreatine shuttle (PCr shuttle). The PCr shuttle ensures that different areas of the cell produce the same amount of force regardless of the mitochondrial distribution. However, our model also shows that when the cellular oxygen supply is limited—as can be the case in conditions such as heart failure—the PCr shuttle cannot maintain uniform ATP and ADP concentrations across the cell. This causes a non-uniform acto-myosin force distribution and non-uniform twitch duration across the cell cross section. Our study suggests that mechanisms other than the PCr shuttle may be necessary to maintain uniform supply of ATP in a hypoxic environment.

Introduction

Cardiomyocytes require a ready supply of adenosine triphosphate (ATP) in order to generate the contractions that cause the heartbeat. ATP demands at hydrolysis sites within myofibrils can vary five-fold between resting and active states of heart [1–3]. Most of this ATP comes from longitudinal columns of cardiac mitochondria, which traverse in between columns of myofibrils. Previous studies have suggested that cardiac mitochondria are arranged in a ‘crystal like’ regular pattern with very small deviation in the distances between neighbouring parallel strands of mitochondria [4, 5]. It was also predicted that this highly ordered mitochondrial arrangement further leads to the formation of functional units called Intracellular energetic units (ICEU) [5–7]. Within the ICEUs, neighbouring mitochondria and myofibrils were proposed to interact via energy transfer mechanisms including phosphocreatine (PCr) shuttle facilitated transport of ATP/ADP, direct diffusion of ATP/ADP as well as adenylate kinase reactions. It was also proposed that the presence of localized diffusion barriers within the ICEUs might lead to limited exchange of ATP/ADP with the larger cytosolic pool of high-energy phosphate compounds (phosphagens) outside the ICEUs [7, 8].

However, these previous studies were based on confocal image data, which did not provide an accurate description of the mitochondrial arrangement. We recently analysed [9] 2D electron microscopy (EM) images of cross-sections covering the entire diameter of the cell from Sprague Dawley (SD) rat hearts. The analysis revealed that cardiac myocytes have a non-crystalline distribution of mitochondria across the cross sections. Individual mitochondria varied in shape, size and exhibited variations in clustering between the myofibrillar bundles. Other recent EM studies [10, 11] also confirm our observations about the heterogeneous distribution of mitochondria in cardiomyocytes. Considering the previously proposed hypothesis of ICEUs, this observed mitochondrial heterogeneity could give rise to a non-uniform distribution of ATP/ADP which can

have a significant impact on the contractile performance of the cell. Furthermore, we [9] and others [11, 12] have reported changes to this heterogeneous distribution of mitochondria as a consequence of changes to mitochondrial substrate selection and metabolism in disease conditions. Thus, it is important to understand how the cell maintains a uniform distribution of ADP, ATP and acto-myosin force production with a heterogeneous mitochondrial distribution.

In this study, we build on our earlier 2D stereological and compartmental model simulation analyses in Jarosz et al [9] and investigate the effect of the mitochondrial distribution displayed in these high-resolution images on the spatial distribution of phosphagens and contractile force dynamics across the cross-section of the cell. We have studied the diffusion of phosphagens within the cell cross section using new, spatially detailed finite element models. Although finite element (FE) based computational models have been used to study the energy landscape in cardiac myocytes previously [13–16], these models defined idealised geometric domains (crystalline mitochondria or rectangular grid-like arrangements) and did not account for the mitochondrial clustering and non-uniform distribution that we observe in our data (Fig 1). The simulations and analyses in our study were conducted using three cross-section images that were selected from different positions within a 3D serial block-face scanning electron microscopy (SBF-SEM) dataset of a single control cardiomyocyte (Fig 1). This allowed us to compare between simulation results from different regions of the cell and to investigate the various structural factors that influence metabolic landscape of the cell.

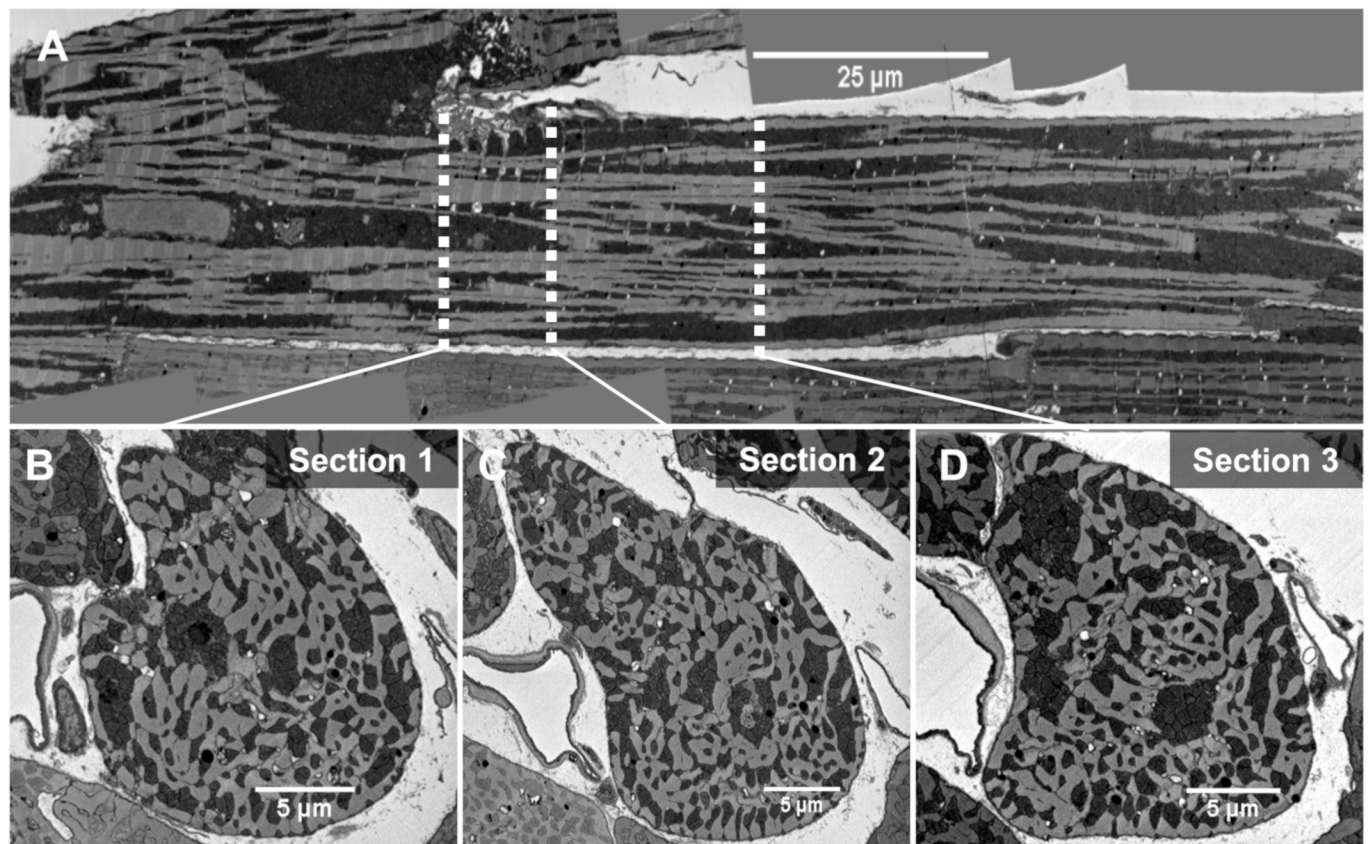


Fig 1. EM image of a single cardiac myocyte. (A): A Longitudinal section from the SBF-SEM images of a single cardiomyocyte with mitochondria in dark regions and myofibril/nucleus in light regions. (B–D): Cross sections (1–3) corresponding to the location of three white dotted lines in the longitudinal section. Section 1 is located near a branching point, and section 2 is located close to a nucleus, however none of the sections contain a nucleus.

<https://doi.org/10.1371/journal.pcbi.1006640.g001>

When investigating how the heterogeneous distribution of mitochondria affects the distribution of ATP, we must also account for the roles that the phosphocreatine shuttle mechanism and oxygen (O₂) supply play in maintaining energy supply within the cell. A uniform supply of O₂ would ensure that each mitochondrion in the cell cross section can accomplish the final stage of oxidative phosphorylation to produce ATP. The phosphocreatine shuttle enables rapid transport of inorganic phosphate from the vicinity of mitochondria to the vicinity of myofibrils, where it is used for muscle contraction in the form of ATP. Models such as [13–16], have only studied the role that phosphocreatine shuttle plays in the context of a uniform or crystalline distribution of mitochondria. To the authors' knowledge no spatially realistic computational model has yet examined how oxygen supply and distribution across the cell cross section (or lack thereof in hypoxic conditions) might also interact with the phosphocreatine shuttle mechanism to facilitate uniform supply of ATP. Specifically, we set out to determine whether the phosphocreatine shuttle mechanism is sufficient to maintain uniform ATP supply across the cross section in normoxic and hypoxic conditions at moderate and high workloads in a heterogeneously distributed mitochondrial environment.

We report several new and important findings based on the computational simulations that we have conducted in this study: (i) The heterogeneous mitochondrial distribution can lead to large gradients in the concentration of inorganic phosphate (Pi), creatine phosphate (PCr) and creatine (Cr) at high workloads when exposed to normal oxygen supply (normoxia) from the capillaries. These large concentration gradients exist over the entire cross-section of the cell between areas with high and low localised mitochondrial density. However, the gradients in ATP and ADP are negligible due to the rapid diffusion of PCr and Cr coupled with the activity of CK enzymes; (ii) regional variation in intracellular oxygen supply can impact the metabolite distribution under hypoxic conditions; (iii) and finally, by computing the cross-bridge dynamics using our simulated metabolite distributions and a prescribed Ca²⁺ transient signal as input, we show that the peak force distribution and twitch duration is insensitive to a heterogeneous distribution of phosphagens under normoxic conditions. However, the twitch duration, defined as the duration when the force is above 5% of peak force, can vary by as much as 30 ms between different parts of the cell under hypoxic conditions.

The following sections present the formulation of the finite element model simulations and the subsequent results that point towards the above-mentioned findings. In the results section, we first analysed the local density of mitochondria within the three cross-sections that were used for this study. We have also provided details of the model formulation along with validation of the model with experimental measurements from previous studies. Following this, we have presented the results from six different sets of simulations based on the three cross-sections under normoxic and hypoxic conditions. We discuss the physiological significance of the presented results, limitations of the current analysis and future directions. Finally, the mathematical formulation of the FE model used in these simulations is described in detail in the material and methods section.

Results

Quantification of mitochondrial distribution in single cell cross-sections

We collected serial block face scanning electron microscopy (SBF-SEM) images of one complete cell [17, 18]. Fig 1A presents a longitudinal section from the 3D dataset, while Fig 1B, 1C and 1D show the cross sections corresponding to the positions marked by the white lines on Fig 1A. The first cross-section in Fig 1B (section 1) was located near a branching point of the cell. On the other hand, section 2 is in the proximity of a nucleus, although none of the three cross-sections contain any portions of the nucleus. As evident from these images, mitochondria were

highly clustered in both lateral and longitudinal sections. In order to quantify the distribution of mitochondria in the cross sections, we used IMOD [19], an open source image processing software package, to segment the cell membrane and mitochondrial cluster boundaries [20] in the three cross sectional images (Fig 2A). Following this, we calculated the local area density of mitochondria (simply referred as mitochondrial density here on) at different points in the images, which is defined as the normalized mitochondrial area ($Area_M$) present inside a square local window ($Area_T$) centred at a given point (Fig 2B). We tested the sensitivity of this measurement to the size of the square window used in the analysis. The difference between the first and third quantile of the mitochondrial density distribution was maximum when a small local window size ($<1 \mu\text{m}$) was used (Fig 2C) and decreasing as the window size increased. Increasing the window size also leads to a decrease in the difference between median of the mitochondrial density distribution and the fractional area of the total mitochondria present in the cross section. However, increasing the window size beyond $1.6 \mu\text{m}$ did not significantly change the median of the distribution, and it also resulted in many outliers (Fig 2C). Therefore, a square window of $1.6 \mu\text{m} \times 1.6 \mu\text{m}$ was used for our analyses (Fig 2D–2F).

We found a significant variation in the mitochondrial density distribution of each cross section (Fig 2D–2F). The first and third quantile of the distribution differs by a margin (IQR) of 20% - 25% in these images. The margin of this difference is lowest in section 2. The star marks inside the boxplots represent the fractional area of total mitochondria present in these sections. Section 2 and 3 have similar area fraction of mitochondria (55%), followed by section 1 (45%).

A high resolution two-dimensional spatial model of cardiac bioenergetics and its validation with experimental results

The descriptions of mitochondrial distribution were incorporated into a 2D finite element (FE) model of cardiac bioenergetics. We first assumed that the distribution of phosphagens within the cardiomyocyte cross sections will be similar across the length of several sarcomeres. We further assumed that individual mitochondria that cluster together share a common inner membrane space (IMS) (Fig 3A). We made this assumption based on a previous EM imaging study by Picard et al. [21], who reported that adjacent mitochondrial outer membranes in cardiac myocytes are connected through electron dense inner-membrane junctions (IMJ). Picard et al. also found a close alignment between the cristae belonging to adjacent mitochondria along the IMJ.

Assuming there is metabolic connectivity between juxtaposed mitochondria, we divided every mitochondrial cluster present in a cross-section EM image into two regions: (i) an IMS region where we implemented partial differential equations (PDE) to simulate diffusion of phosphagens; (ii) and a mitochondrial matrix region with negligible metabolite diffusivity (Fig 3B). The mitochondrial matrix reactions associated with oxidative phosphorylation (OXPHOS) were simulated using an ordinary differential equation (ODE) model developed by Beard [22]. This model had explicit biophysical descriptions of the electron transfer chain, ATP synthase and substrate transport, but a phenomenological relation for the dehydrogenase flux from the TCA cycle. The Beard et al. ODE model was solved at each computation node on IMS regions and coupled with PDEs for metabolite diffusion within the IMS region. As such, we developed a FE mesh from EM images of section 2 using this protocol (Fig 3C).

We assumed a uniform distribution of various enzymes like cytosolic creatine kinase enzymes, adenylate kinase and contractile proteins over the myofibril region within the FE mesh. The equations describing ATP consumption in the myofibril was modelled as a Michaelis–Menten

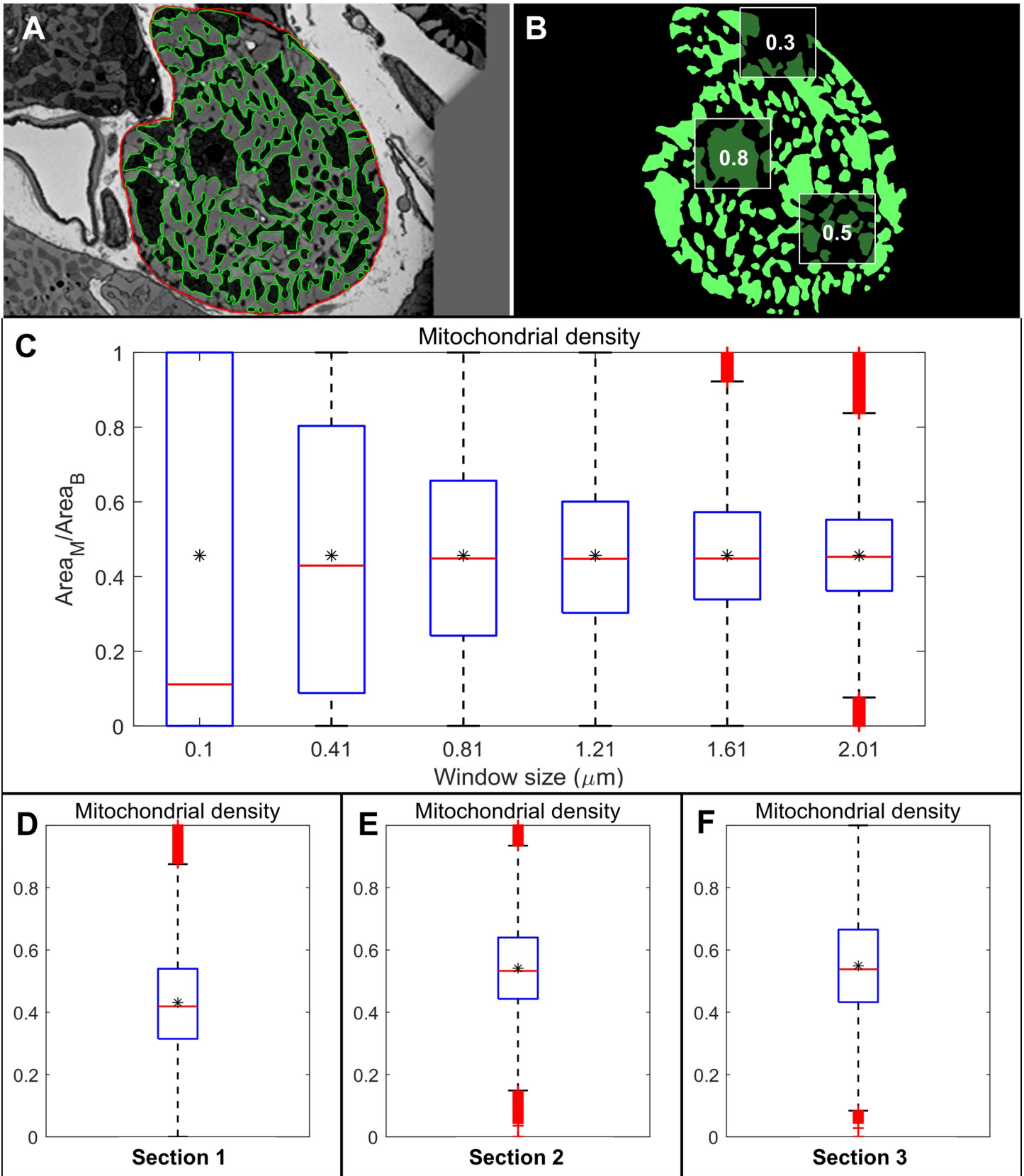


Fig 2. Analysis of mitochondrial distribution in different cross-sections. (A) Cross-section 1 with mitochondria segmented in green and sarcolemma in red. (B) Square windows representing the ratio of mitochondrial area vs myofibrillar area present inside these windows (C) Statistical box plots of the distribution of these ratios corresponding to different sizes of the square windows. The star in the middle of box plots represents the area fraction of total mitochondria present in section 1. (D-F): Box plot representing the distribution of mitochondrial density at various points in the cross-section 1–3. The stars represent the total mitochondrial area fraction present in each cross section. Mitochondrial area fraction is 55% in section 2 and 3 and 45% in section 1.

<https://doi.org/10.1371/journal.pcbi.1006640.g002>

function previously developed by Wu et al [23].

$$V_{ATPase} = \frac{X_{ATPase}}{1 + R \frac{[Pi_C] * [ADP_C]}{[ATP_C]}}$$

Here, $[Pi_C]$ denotes the cytosolic concentration of inorganic phosphate, R is a constant mass-action ratio and X_{ATPase} is a model parameter that can be varied to simulate steady state ATP consumption at various workloads. In order to simulate the action of enzymes such as adenylate kinase and various cytosolic (M-CK) and mitochondrial (mt-CK) creatine kinases, the model also incorporated equations describing the enzyme kinetics from a reaction-diffusion model of cardiac energy transfer described in [13].

We modelled free diffusion of Pi, PCr and Cr between the shared IMS region and the myofibrillar region in the segmented images. On the other hand, diffusivity of ATP, ADP and AMP were set to a value 1% of that in the IMS region, compared to their cytosolic values. This

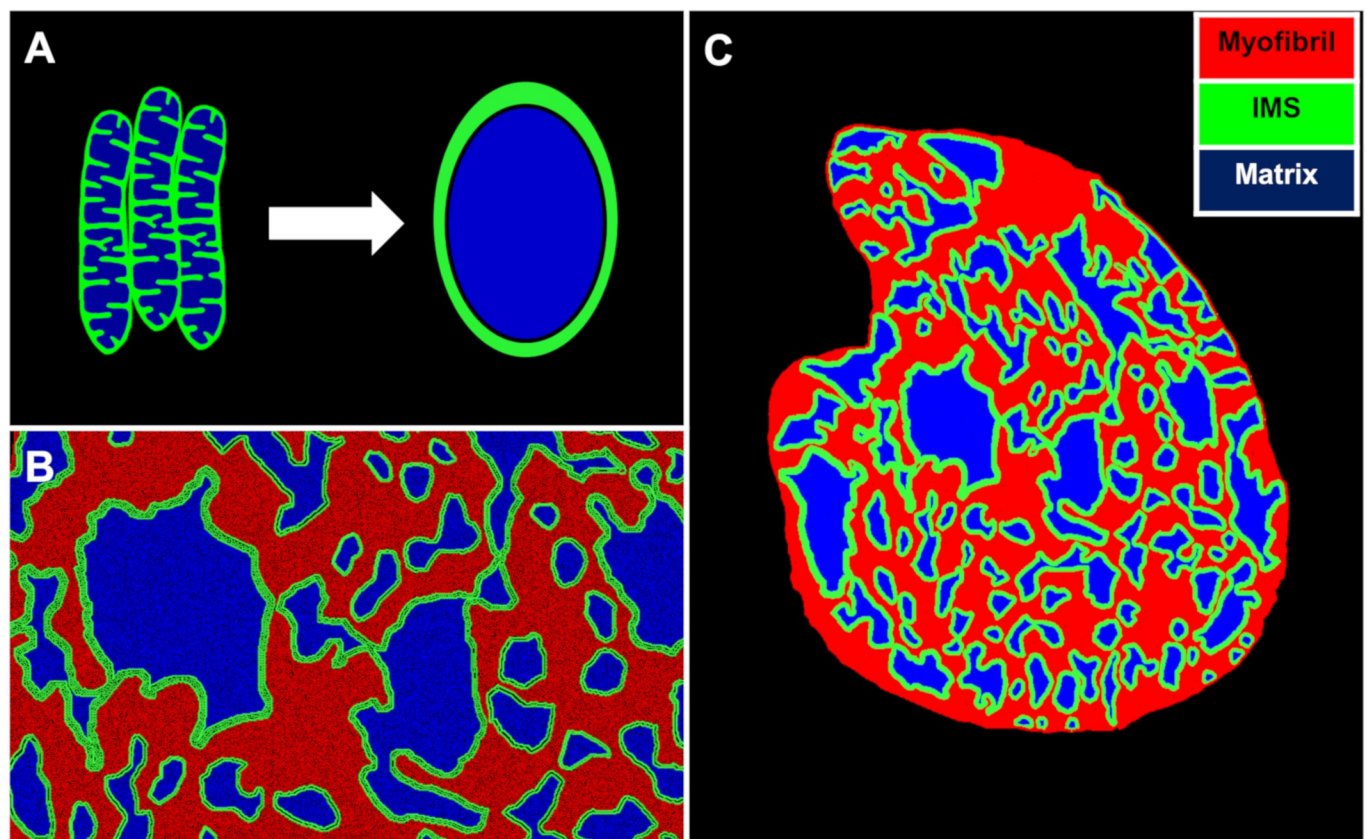


Fig 3. Model assumptions and FE mesh generation from EM image cross-sections. (A): We assumed that individual mitochondria that cluster together will share a common inner membrane space. (B): Based on this assumption, each mitochondrial cluster was divided into two regions: an IMS region, depicted in green and a matrix region, depicted in blue. A third region depicted in red covers the myofibrils present in the cell. (C): Image of a FE mesh developed from the EM image of cross-section 1 with the three different regions.

<https://doi.org/10.1371/journal.pcbi.1006640.g003>

was done to simulate low permeability of the VDACs (voltage depended anion channels) to these large anions as suggested by previous studies [13, 24, 25]. We also assumed that none of these large molecules can diffuse through the mitochondrial matrix due to intramatrix barriers like cristae structure and protein complexes [26].

Owing to its small molecular size, O_2 was assumed to diffuse through the mitochondrial matrix with similar diffusivity as the myofibrils and IMS. Therefore, O_2 was modelled as a species diffusing equally through all the three regions of the EM images. We imposed a constant Dirchlet boundary condition of O_2 in the cell membrane to simulate the O_2 flow from a capillary into the cell. All the other diffusing species in the model were subjected to a no flux Neumann boundary condition at the cell membrane.

We further utilized a thermodynamically-consistent and energy-metabolite-sensitive model of cross-bridge cycling previously developed by Tran et al [27] to predict the force generation at different points in the myofibril area based on the concentration of the following phosphagens: ATP, ADP and Pi. The overall model was solved using the finite element method. A detailed description of the model formulation and choice of various parameters and initial/boundary conditions can be found in Supplementary Material (S1 Text).

Before using our model to predict the metabolic landscape of the cells, we validated the phosphocreatine shuttle and substrate feedback mechanism that we have implemented in our model. Previously, Vendelin et al.'s [13] compartmental model of a rat heart cell suggested that PCr/ATP ratio remains effectively constant over low and moderate workloads but declines significantly at high workloads (Fig 4A). As evident from Fig 4A, our model was able to reproduce similar behaviour for different levels of O_2 consumption. The temperature in our model is the same as that used in the study by Vendelin et al. (298 K). Vendelin et al. validated their model predictions of PCr/ATP ratio by comparing them with experimental PCr/ATP ratio values which were collected from in vivo NMR spectroscopy on several canine hearts [28]. We have also reproduced this data in Fig 4A for comparison with our model predictions. As evident from the figure, our model predictions were consistent with the experimental PCr/ATP ratios from canine hearts.

Our model also predicted a parabolic relationship between average cytosolic ADP concentration vs V_{O_2} , similar to the prediction from Vendelin et al.'s computational study (Fig 4B). These results indicate accurate modelling of the mechanism of substrate feedback between the mitochondria and myofibrils. The V_{O_2} value of 100 $\mu\text{mol}/\text{min}/\text{g}$ tissue in the plot corresponded to a high workload level of $X_{ATPase} = 0.05 \mu\text{M}/\text{sec}$. According to Vendelin et al.'s study [13], this V_{O_2} value also corresponds to around 60% of the maximal filling rate of isolated rat heart perfused according to the "working heart" protocol of Neely [3]. Therefore, we have used $X_{ATPase} = 0.05 \mu\text{M}/\text{sec}$ to simulate high physiological levels of workload in all the subsequent simulations.

In order to make accurate predictions about spatial variation in metabolite concentrations or reaction rates, the model needs additional validation with experimental results, where spatial distributions of diffusing species in the cells have been measured using live imaging techniques (i.e. fluorescence microscopy). In a previous study, Takahashi et al [29] visualised intracellular gradients of myoglobin oxygen saturation using high spatial resolution spectrophotometry and further converted the observed oxygenation level into partial pressure of O_2 (PO_2) using linear regression of data and the Hill equation. Fig 4C represents a comparison between Takahashi et al's data and model estimations for radial profile of PO_2 inside an isolated rat cardiomyocyte. In the experiment, individual cells were subjected to a superfusing O_2 pressure of 15.2 mmHg under a high O_2 consumption rate at room temperature. We simulated high O_2 consumption in a similar range in cross section 1. Subsequently, the model predicted image of PO_2 profile was reduced in resolution and convolved with a confocal microscope point-spread-function to

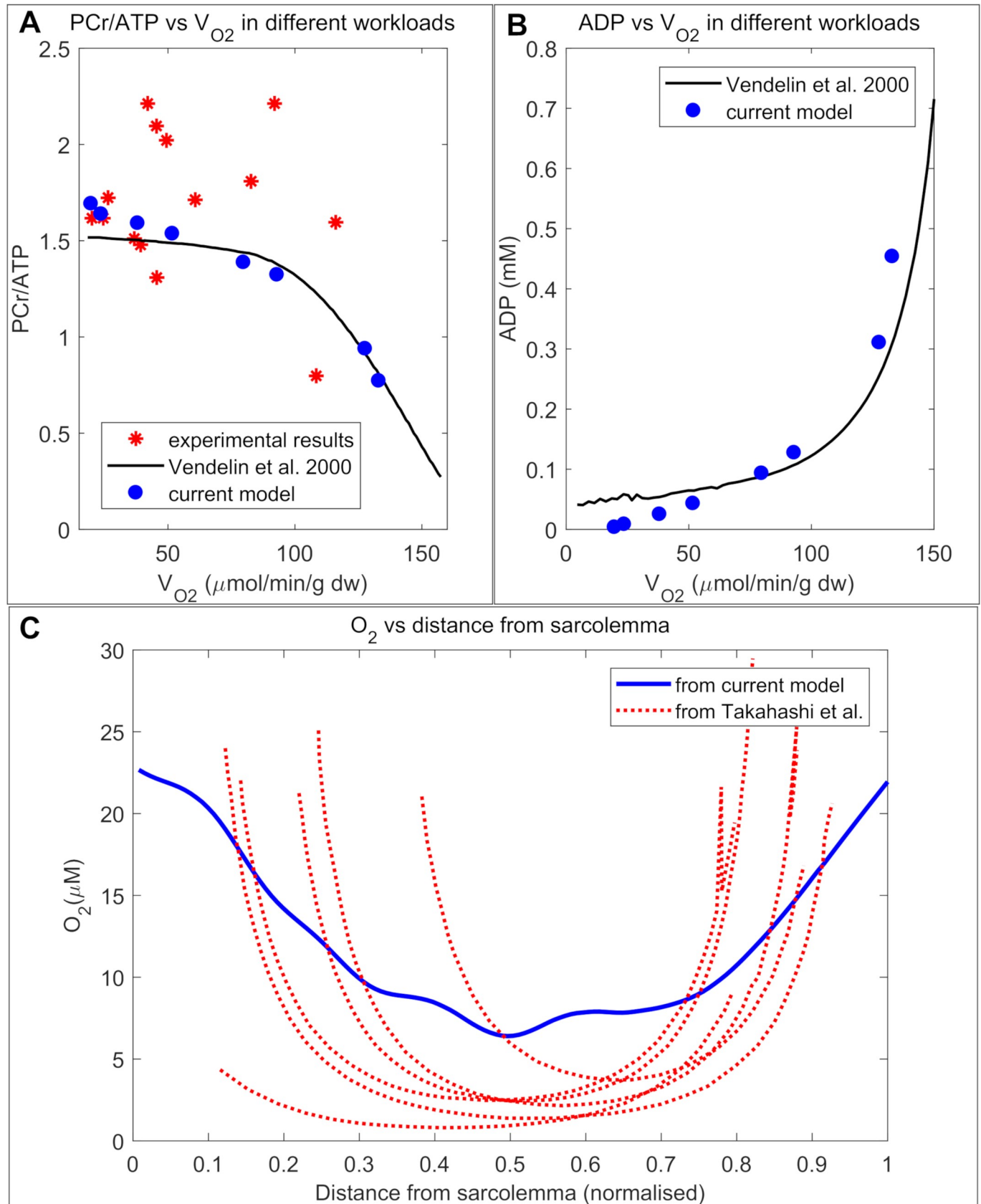


Fig 4. Model validation with experimental results. (A): Comparison between our model-predicted, spatially averaged PCr/ATP ratio vs V_{O_2} with model predictions from Vendelin et al. [13] and experimental results from Valdur Saks et al. [28] (B): Comparison between our model predictions for spatially averaged ADP vs V_{O_2} with predictions from Vendelin et al.'s [13] zero dimensional model (C): Comparison between model predicted radial profiles of O_2 with intracellular PO_2 levels calculated by Takahashi et al. [29] in six different isolated cells.

<https://doi.org/10.1371/journal.pcbi.1006640.g004>

generate a simulated confocal image (S1 Fig), similar to a previous study [30]. Fig 4C shows that the concentration profile in the simulated confocal image of O_2 distribution follows a similar profile to the radial PO_2 gradient experimentally measured by Takahashi et al. [29]. Both the model and experimental measurements demonstrate steep concentration gradients proximal to the sarcolemma and shallow gradients within the cell interior.

The overall analysis presented in Fig 4A–4C illustrates that our model successfully reproduces both the whole-cell averaged and spatially profiled experimental results described in literature.

Heterogeneous mitochondrial distribution leads to large gradients in metabolite concentration across the cross-section of the cell

Following model validation with the simulation results from cross-section 1, we used the same protocol to simulate cardiac energy metabolism in the three cross sections presented in Fig 1B–1D under a high workload ($V_{O_2} = 100 \mu\text{mol}/\text{min}/\text{g}$ tissue). It was assumed that the cell is exposed to a normal oxygen pressure from capillaries, and the concentration of O_2 at the sarcolemma was maintained at $45 \mu\text{M}$ based on Mik et al.'s experimental study [31].

Profiles of cytosolic ADP/ATP ratio, Pi and ATP hydrolysis rate (J_{ATPase}), corresponding to these cross sections (Fig 5) show significantly large gradients ($600\text{--}1000 \mu\text{M}$) of Pi concentration across the cell. On the other hand, ATP and ADP show spatial gradients in the order of $10 \mu\text{M}$, which is small compared to the average ADP level (approximately $100 \mu\text{M}$) and negligible compared to the average ATP level (approximately 10mM). The ATP hydrolysis rate, being a function of both Pi and ADP/ATP, varies by a margin larger than the ADP/ATP ratio variation but lower than the gradients of Pi. By comparing the different cross-sections (Fig 5), we also observe that section 1 has a higher average level of ADP and Pi compared to the other two sections for the same cytosolic X_{ATPase} activity. Section 2 and 3 also show a larger gradient in the V_{ATPase} . These differences can be explained by the lower mitochondrial area fraction of section 1 as shown in Fig 2D. Although section 1 is closer to section 2 than section 3 ($12.5 \mu\text{m}$ vs $25 \mu\text{m}$ of longitudinal distance), section 1 is located near a branching point of the cell unlike the other two sections. Besides similar average values, cross-sections 2 and 3 also have very similar spatial profiles of Pi. The Pi concentration is higher in the upper corner of these cross sections and it gradually increases towards the lower left of the sections. These results are consistent with our initial assumption of symmetric metabolic landscape between different cross-sections of the cell.

In the Fig 6A we have presented a boxplot of the model predicted gradients of all the diffusing metabolite levels present in cross section 1. The differences in spatial gradients of phosphagens can be attributed to the activity of creatine kinase (CK) enzyme isoforms in the IMS and myofibrils. Based on previous work by Vendelin et al [13, 25], we assumed ADP, ATP and AMP diffusivity in the IMS region is 1% of their corresponding diffusivity in the cytosolic space. Despite restricted diffusivity, the estimated ADP and ATP gradients were less than one tenth of the gradients present in PCr and Cr (Fig 6A). These results point towards the significance of the cytosolic MCK enzyme reaction, which acts as a spatial buffer of the ADP/ATP ratio by converting excess ADP into ATP at the cost of the PCr reserve of the cell. We contrasted the PCr and Cr concentration at different regions of cross section 1 with the corresponding

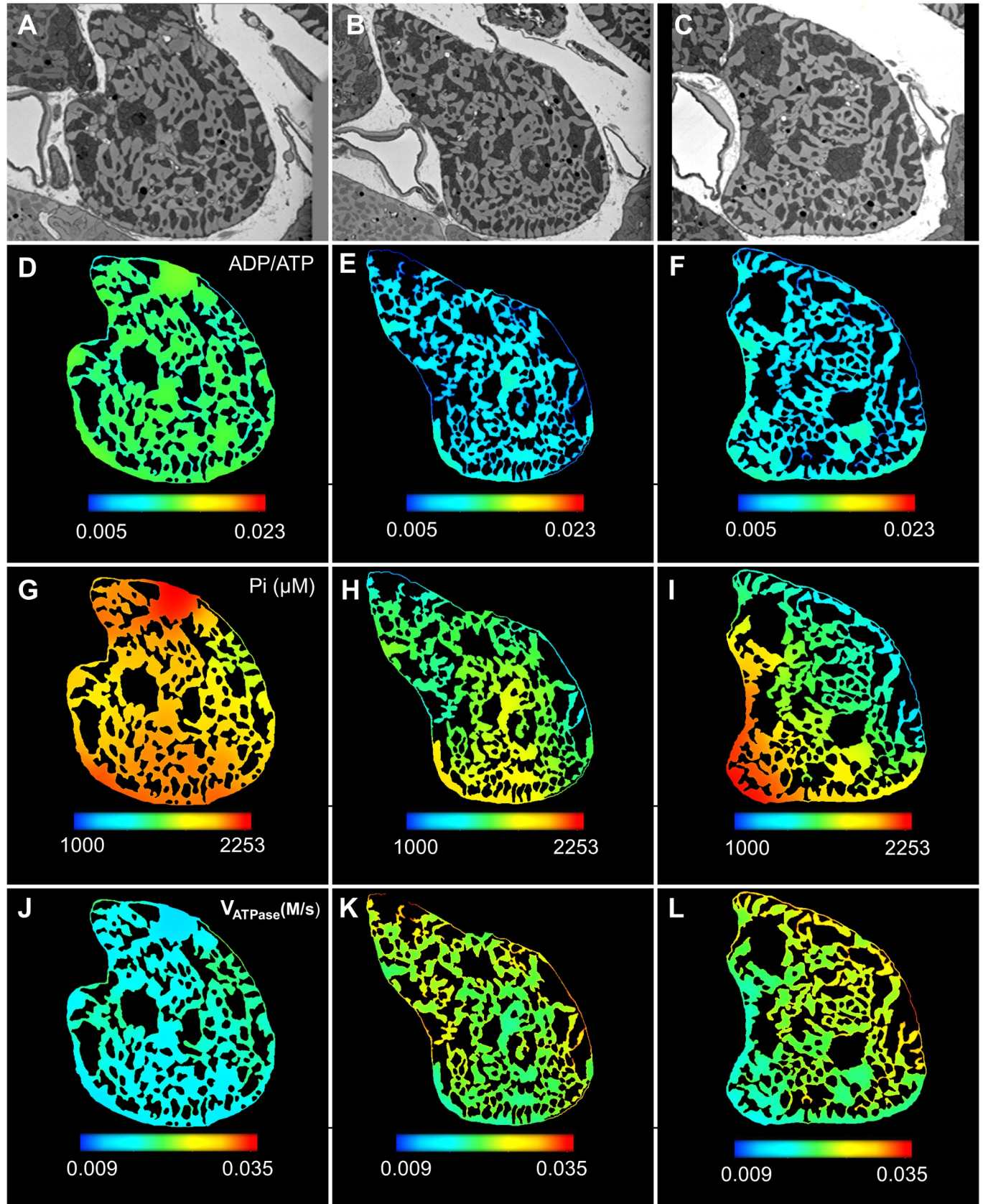


Fig 5. Spatial variation in model predicted cytosolic phosphagen levels and reaction rates represented using colour spectrum. All the figures were generated by using the same range of colour spectrum for a particular phosphagen. (A-C): EM images of sections 1–3 (D-F): Distribution of ADP and ATP in the cross-sections represented using the ADP/ATP ratio. The ADP/ATP ratio remains uniform throughout the cross-sections (G-I): Inorganic phosphate (Pi) shows large spatial variation at the order of 1 mM. (J-L): Spatial variation in the ATP hydrolysis rate in the myofibrils corresponding to $X_{ATPase} = 0.05 \mu\text{M}/\text{sec}$.

<https://doi.org/10.1371/journal.pcbi.1006640.g005>

local mitochondrial density (Fig 6B). This model predicts that myofibril regions with lower mitochondrial densities contain a lower reserve of PCr. The model predictions are also consistent with the accepted role of the PCr shuttle, in facilitating a rapid metabolic exchange of the equivalent energy of ATP between the IMS and myofibrils.

Force dynamics is insensitive to heterogeneity in concentration of phosphagens and distribution of mitochondria

To analyse the impact of the spatial distribution of energy phosphagens on mechanical force production, we have used Tran et al.'s [27] cross-bridge cycling model to simulate isometric twitches at each of the discretised nodes. The isometric twitches are activated by a prescribed Ca^{2+} transient. It was assumed that the average value of various metabolite concentrations remains unchanged during a twitch, and accordingly the behaviour of the cross section was modelled as a function of cytosolic ATP, ADP, Pi, MgATP, MgADP and pH. The peak twitch force (F_{peak}) was simulated (Fig 7A–7C) for the cross sections, as were twitch durations (Fig 7D–7F), defined as the duration that the force was above 5% of F_{peak} (t_{95}). F_{peak} shows slight spatial variation in sections 2 and 3 (~7% difference between maximum and minimum spatial values), while it is almost uniform across section 1 (<3% difference). Similarly, differences between the maximum and minimum values of t_{95} is around 12% in section 2 and 3, while it is around 5% in cross-section 1. These results imply that the force production is relatively insensitive to the large gradients in inorganic phosphate observed in Figs 5 and 6. The results also predict that rapid diffusion of PCr and Cr, coupled with CK enzyme reactions in myofibrils and IMS, is sufficient to maintain a uniform force generation across the cell cross section despite the heterogeneous distribution of mitochondria.

Diffusion of PCr & Cr is not sufficient to maintain uniform force dynamics under hypoxic conditions

According to previous studies [32, 33] on isolated rat cardiomyocytes, cardiac energetics is impacted when the extracellular O_2 diminishes below a margin of 20 μM , as the mitochondrial oxidative phosphorylation system is limited. In an in-vivo non-invasive study on wistar rat hearts [31], Mik et al. found an average PO_2 of 35 mm Hg (roughly equivalent to 45 μM concentration assuming an O_2 solubility coefficient $1.35 \times 10^{-6} \text{ M}/\text{mmHg}$ [34]) present over the surfaces of cardiac mitochondria, which is well above this margin. However, Mik et al. also found that a significant percentage (25%) of in-vivo mitochondria was exposed to PO_2 in the range of 10–20 mm Hg under normal O_2 supply. Reducing the O_2 supply to the heart resulted in an even larger fraction of cardiac mitochondria (40%) with low surface PO_2 in the range of 0–10 mm Hg. Mik et al.'s findings were consistent with predictions from previous modelling studies by Beard et al. [34] and Groebe et al. [35]. Both modelling studies predicted that cardiac myocytes in-vivo can be exposed to a variety of PO_2 depending on location of the cells relative to capillary networks.

Therefore, we investigated the effect of low oxygen on phosphagens distribution in the 2D cross-sections. As shown in the previous results, we first applied a Dirichlet boundary condition with O_2 concentration of 45 μM along the cell membrane, which represents the majority of cells present in heart. In the second simulation we imposed a 15 μM oxygen concentration

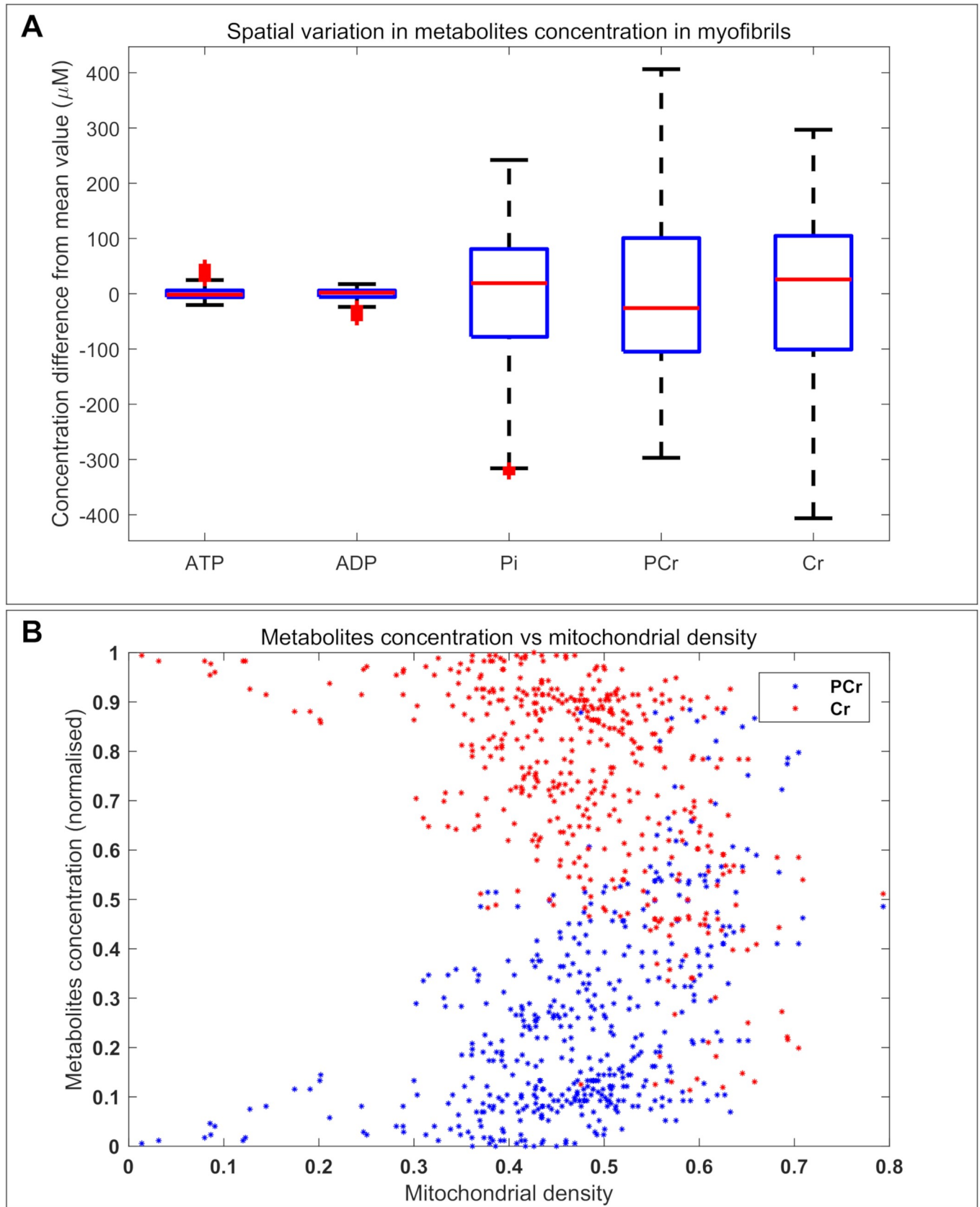


Fig 6. Spatial variation in phosphagens concentration in cross section 1. (A): Phosphagen concentrations were calculated at all the myofibril points in the mesh and subtracted from the spatially averaged concentration of each phosphagen ($Phosg_{ave}$). Box plots represent the statistical distribution of the difference between phosphagen concentration at each point and $Phosg_{ave}$ value of each phosphagen. The zero value corresponds to the $Phosg_{ave}$. (B): Normalized concentration of PCr and Cr displayed as a function of local mitochondrial density at various points in the cell. PCr and Cr concentrations were normalized by a factor equivalent to the difference of PCr and Cr maximum and minimum concentrations in cross section 1.

<https://doi.org/10.1371/journal.pcbi.1006640.g006>

along the cell membrane, representing the cells exposed to lower levels of oxygen supply (hypoxic condition). Both the simulations corresponded to the same high workload levels.

Profiles of O_2 concentration in the cardiomyocyte, corresponding to these two simulations, are shown in Fig 8A. In both the cases, the O_2 distributions show steep gradients from the sarcolemma. While in the first case O_2 concentration remains above $20 \mu M$ throughout the cell, our model predicts an anoxic cell core under hypoxic conditions. This prediction is consistent with observations of Takahashi et al. [29, 36] on isolated cardiomyocytes as well as Mik et al.'s study [31] on mitochondria in the in-vivo heart. To better understand the effects of an oxygen deprived cell core on mitochondrial electron transfer system (ETS), we have plotted the mitochondrial complex IV reaction rate (V_{C4}) as a function of the IMS space (Fig 8B). Complex IV is the main site of oxygen consumption in the ETS. As expected in normoxia, activity of V_{C4} is nearly uniform across the cell cross section, with small variations due to mitochondrial cluster sizes. However, in the hypoxic simulation, a negligible amount of O_2 passes to the interior of the cell, which in turn inhibits the J_{C4} .

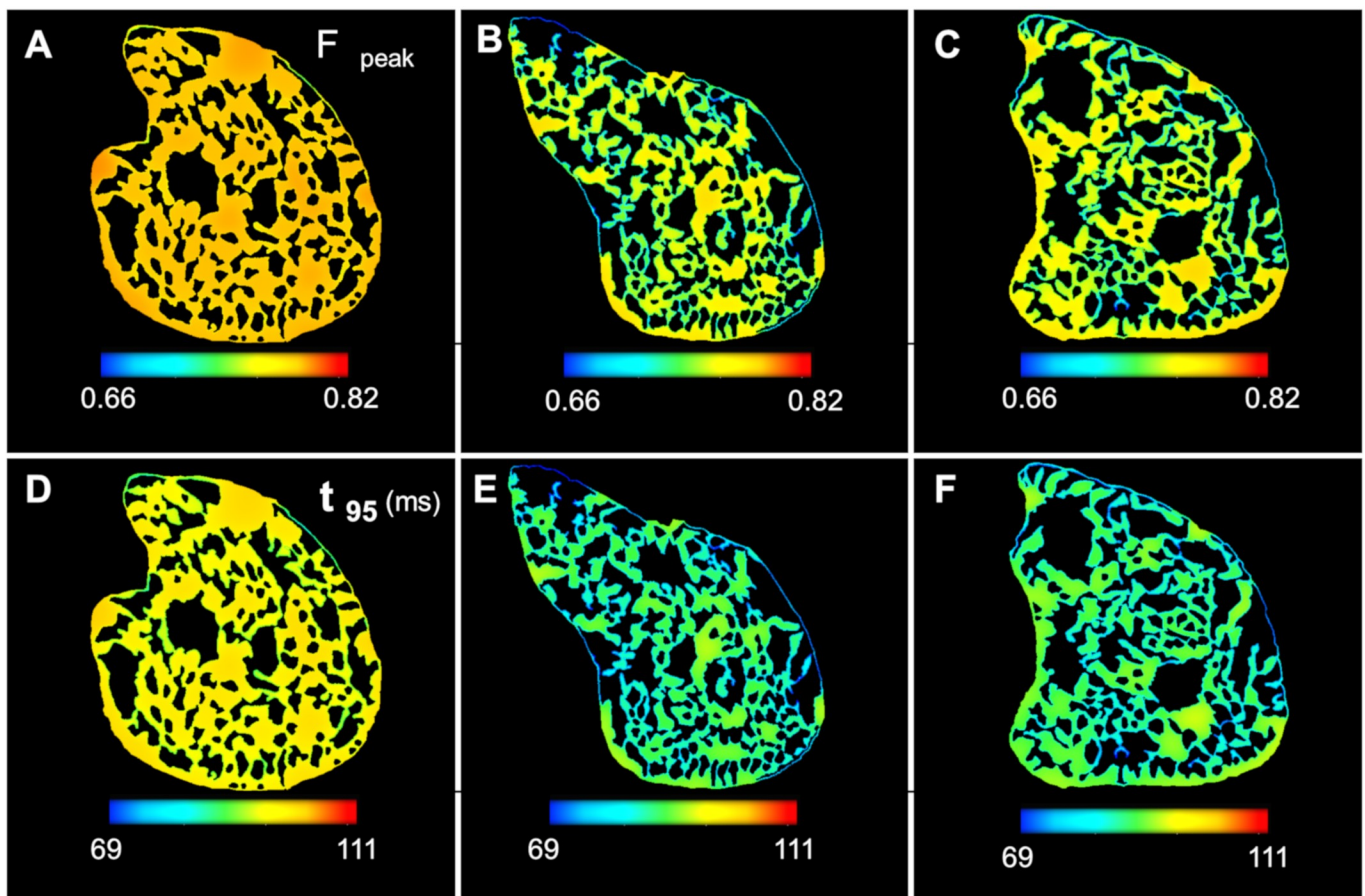


Fig 7. Force dynamics of the cell corresponding to the model predicted phosphagens distribution. (A-C): F_{peak} is uniform across section 1 and exhibits slight spatial variation in section 2 and 3. (D-F): t_{95} shows similar spatial gradients across the cross sections.

<https://doi.org/10.1371/journal.pcbi.1006640.g007>

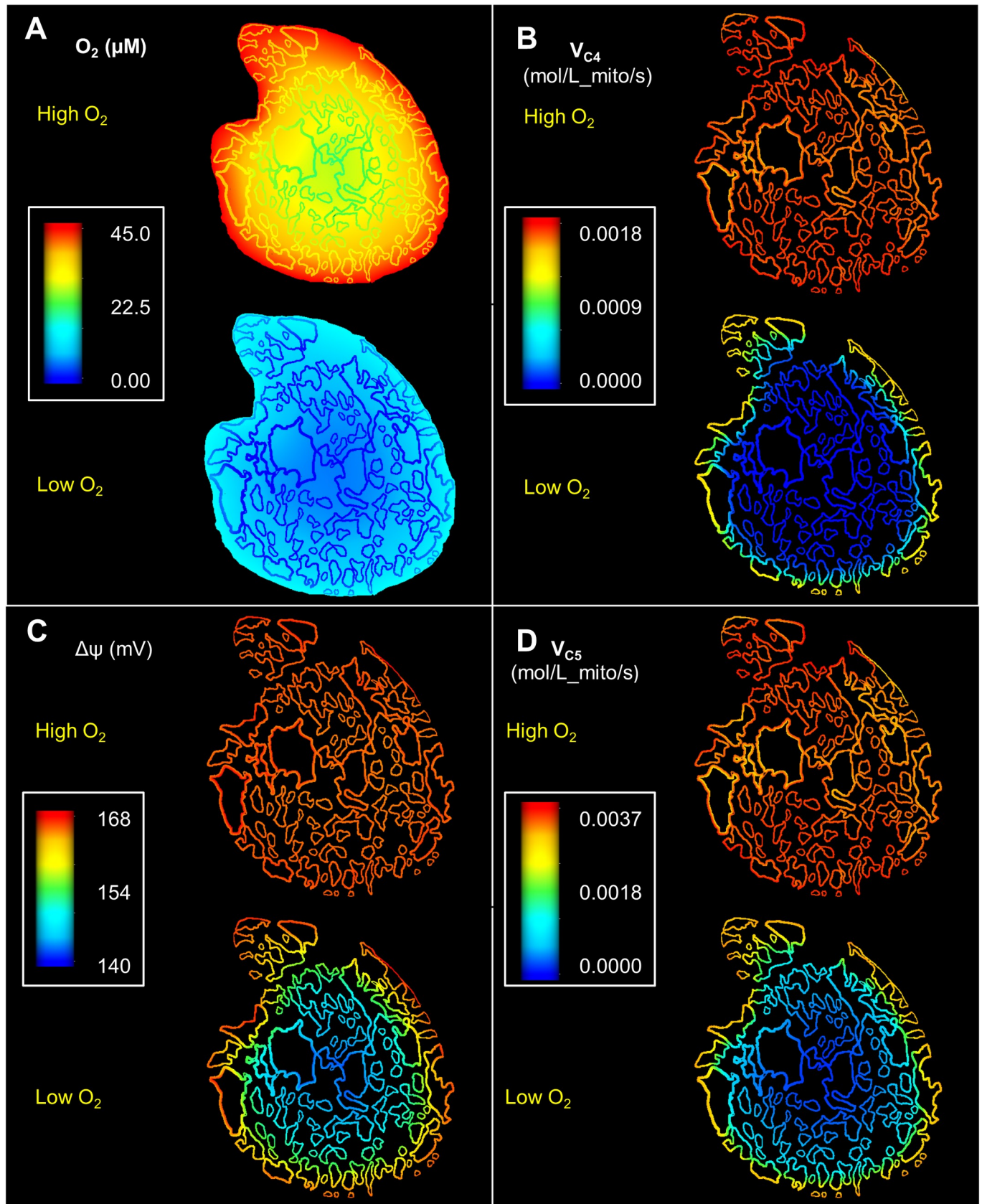


Fig 8. Spatial variation in model predicted mitochondrial reaction rates and O₂ profiles for cross section 1. All the figures were generated by using same colour spectrum range. (A): Steady state O₂ profiles showing steep O₂ gradients in the vicinity of the sarcolemma. In the hypoxic case, it also leads to the formation of an anoxic core with negligible O₂ level (B): The reduction of oxygen at complex IV is inhibited in hypoxia, while it is uniform across the section in normoxia. (C): Hypoxia leads to a steep gradient in the model predictions for mitochondrial membrane potential (D): Under normoxia Complex V (F₁-F₀ ATP synthase) reaction rate is nearly uniform across the cell with slight variation near the larger mitochondrial clusters. However, ATP synthesis at Complex V is inhibited in the anoxic core under hypoxia.

<https://doi.org/10.1371/journal.pcbi.1006640.g008>

We also investigated the influence of intracellular O₂ profiles on mitochondrial membrane potential ($\Delta\psi$) for both the normoxic and hypoxic simulations (Fig 8C). In the first case, $\Delta\psi$ was nearly uniform across the cell. This uniform distribution of $\Delta\psi$ is clearly in accordance with the uniform profile of V_{C4} observed in Fig 8B. However, in the second case, $\Delta\psi$ is significantly depressed in the core of the cell. This spatial depression of $\Delta\psi$ can be attributed to the decreased ETS flux in the centrally located IMF mitochondria. The lower row in Fig 8D demonstrates the effect of this depression in $\Delta\psi$ on reaction flux of complex V. The rate of ATP synthesis at complex V follows the same spatial profiles as $\Delta\psi$. As a result, ATP synthesis declines in the centre of the cell in hypoxia.

The diminished rate of ATP synthesis in the mitochondria at the core of the cell also had a significant impact on transportation of ATP/ADP through the phosphocreatine shuttle (Fig 9). For instance, the reaction rate of mtCK in the forward direction ($\text{ATP} + \text{Cr} \rightarrow \text{PCr} + \text{ADP}$) was around 15% lower in the central parts of the cell compared to the periphery under hypoxia (Fig 9A). As a result, the model predicts a strong radial gradient in the ADP/ATP ratio (Fig 10A) in the hypoxic simulations. This contrasts with the simulations of normoxic situation where both the mtCK reaction rates and the ADP/ATP ratio shows negligible spatial variation (Figs 9A and 10A). Fig 10B similarly demonstrates a radial profile in the ATP hydrolysis rate for the second case. The abundance of ADP in the anoxic cell core also leads to an elevated cytosolic MCK reverse reaction rate ($\text{PCr} + \text{ADP} \rightarrow \text{ATP} + \text{Cr}$) which is substantially higher in the anoxic core compared to the periphery of the cell (Fig 9B). Together these results suggest that activity of mtCK and MCK is not sufficient for maintaining uniform ADP/ATP under limited O₂ supply.

For the second simulation, F_{peak} is also higher in the anoxic core of the cell (Fig 10C) and the twitch durations are significantly longer (Fig 10D). The difference between the maximum and minimum spatial values of t_{95} is around 23% in the second simulation compared to only 5% in the first simulation. This is a result of lower ATP, and higher ADP and Pi in the centre of the cell—which slows down the cycling rate, but at the same time, the cross bridges spend more time in the force-producing states (due to lower ATP), leading to higher force development. This result is consistent with several experimental studies [37, 38] as well as a recent modelling study by Tewari et al. [39] which suggests that force production increases with increasing ADP and decreasing ATP levels.

A consequence of having longer twitch durations is that at high stimulus frequencies, the twitch does not have time to completely relax resulting in a higher diastolic force. Thus, according to the model predictions, different regions of the same cell cross section will be experiencing different levels of force in both systole and diastole. This may lead to shear strain inside the cell and wastage of metabolic energy through production of heat—which might not be a favourable situation during a high cardiac workload. The effect of contraction on the cellular ultrastructure was not considered in the model. Contraction of the cell can change the cell dimensions, particularly by increasing the cell cross section area due to conservation of volume. If the hypoxic cell core is contracted longer due to a reduction in ATP, it is likely to lead to an increase in the average diffusion distance between the cell core and the cell periphery. Increases in diffusion distance can lead to a further decrease in the supply of ATP in the

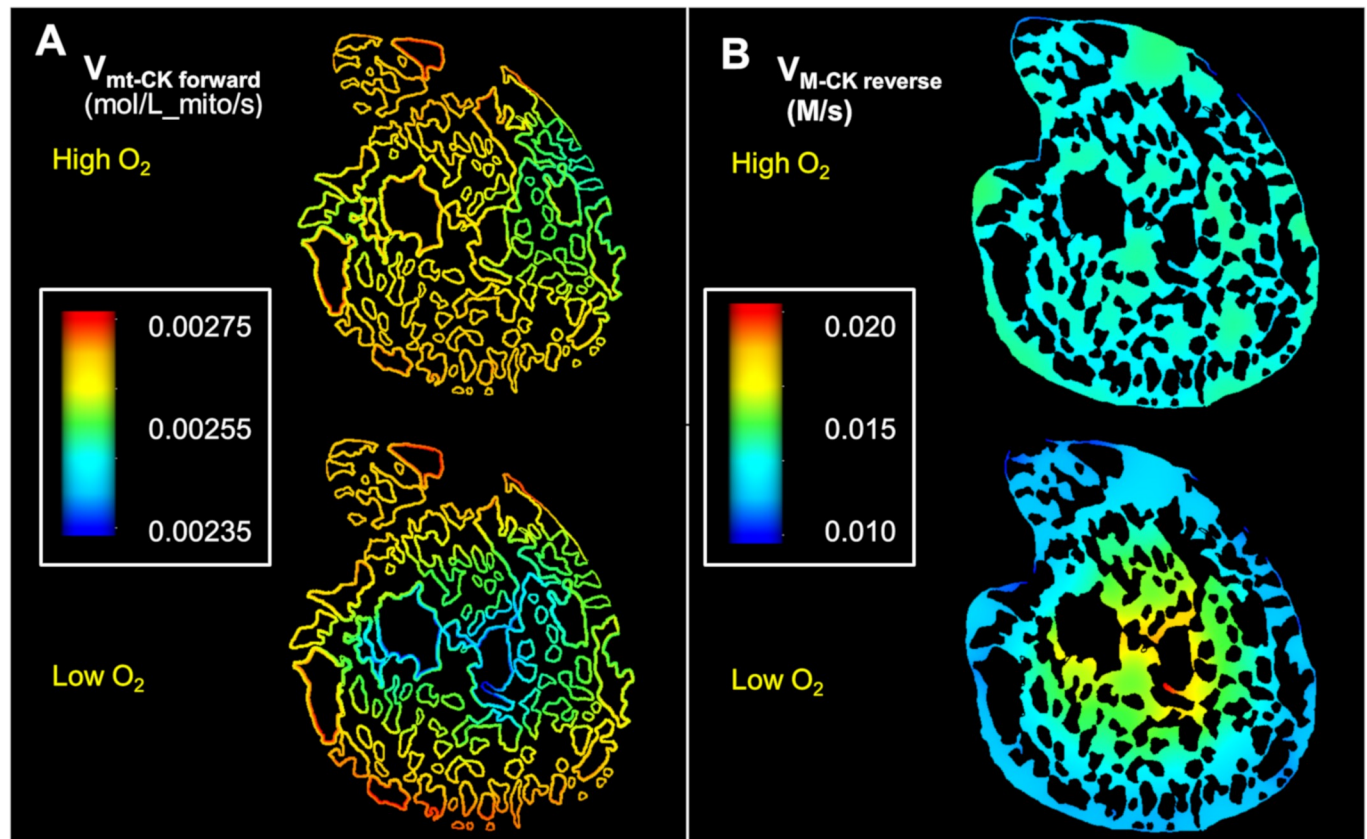


Fig 9. Spatial variation in rates of CK enzymatic reactions involved in phosphocreatine shuttle under normoxia and hypoxia. All the figures were generated by using same colour spectrum range. (A): Steady state profiles of reaction rates of mitochondrial mtCK in forward direction ($\text{ATP} + \text{Cr} \rightarrow \text{PCr} + \text{ADP}$) (B): Steady state profiles showing reaction rates of myofibrillar MCK in reverse direction ($\text{PCr} + \text{ADP} \rightarrow \text{ATP} + \text{Cr}$).

<https://doi.org/10.1371/journal.pcbi.1006640.g009>

hypoxic cell core—thus creating a negative feedback loop that might contribute to irreversible contraction of the cell.

These results imply that unlike under normoxic conditions, diffusion of Cr and PCr and associated CK enzyme activities is not sufficient to maintain a uniform ATP/ADP concentration and force dynamics under hypoxic conditions.

Discussion

Distribution of phosphagens in cell cross-sections

We have developed a computational model of cardiac bioenergetics based on EM images to study the impacts of the heterogeneous distribution of mitochondria on the energy metabolic landscape of the cell. Note that this differs markedly from the earlier held concept that cardiomyocyte mitochondria are arranged within rigid crystalline lattice networks, which is thought to enhance diffusion and exchange of compounds such as the phosphagens. When less structured mitochondrial arrangements are incorporated into models, our results reveal that significant gradients in the phosphagen concentrations are likely. While concentration gradients are currently difficult to observe directly in experimental studies, previous computational studies, defined over idealised crystal lattice-like geometries, predicted smaller concentration gradients between adjacent mitochondria and myofibril units. Our current study indicates that significant concentration gradients may occur over the entire cross-sectional area of the cell, that this

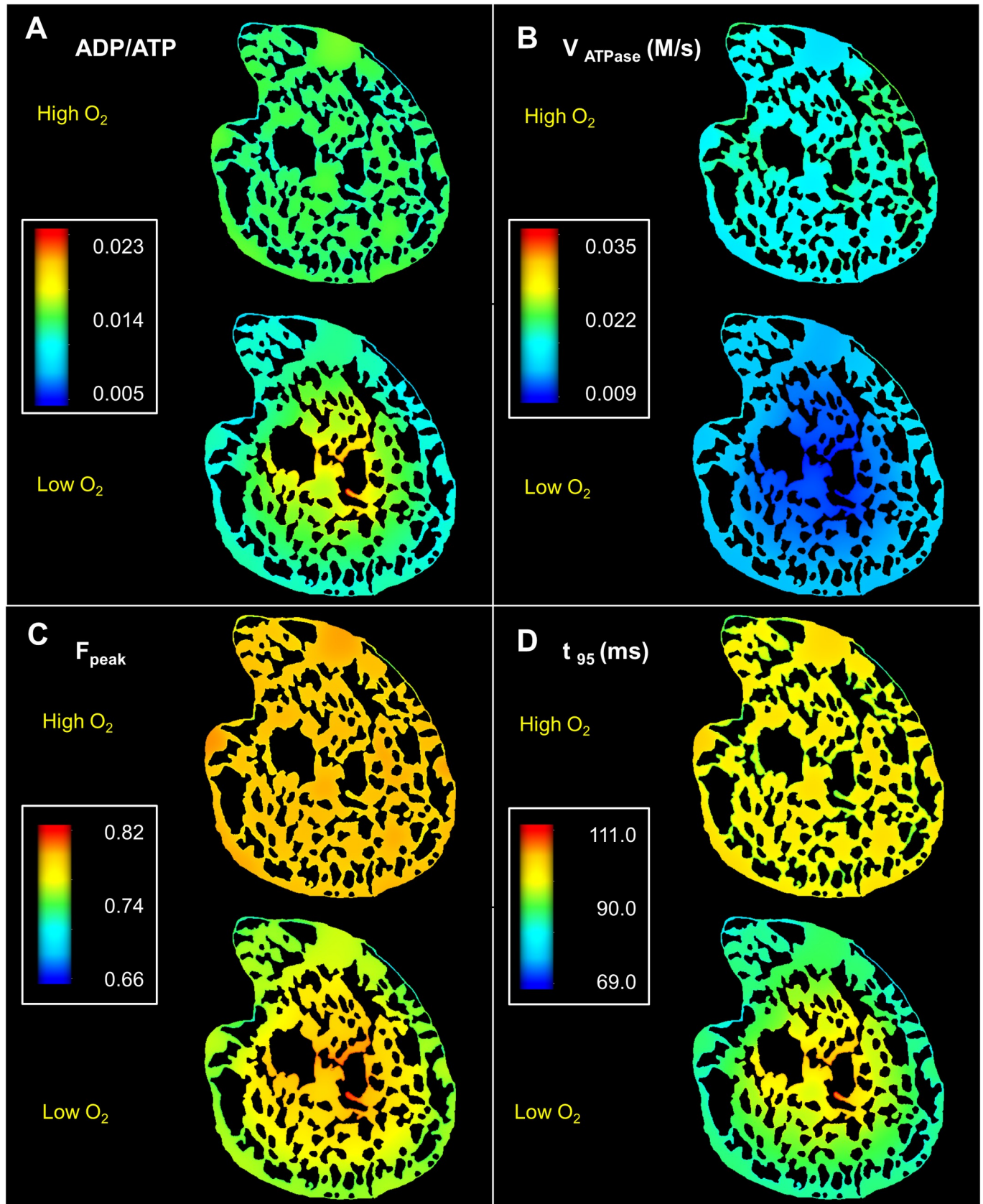


Fig 10. Spatial variation in cytosolic metabolite concentration and force dynamics under normoxia and hypoxia. (A): Steady state profiles of ADP/ATP ratio. ADP/ATP is significantly higher in the anoxic cell core under low O₂ supply (B): ATP hydrolysis rate is similarly lower in the cell core under hypoxic condition (C): Peak twitch force (F_{peak}) is significantly higher in the cell core under hypoxia (D): Increased F_{peak} is complemented by increased twitch duration in the cell core, which can lead to loss of energy in the form of shear strain.

<https://doi.org/10.1371/journal.pcbi.1006640.g010>

is dependent on local mitochondrial densities at a given point in the cell, and that these gradients appear acutely sensitive to hypoxia, such as would occur in infarcts.

Distribution of phosphagens along the longitudinal axis of cell

Our model was based on 2D cross sectional images, but we expect similar results if a 3rd dimension along the longitudinal axis of the cell is added to the model. To elaborate, Figs 5 and 6 shows that spatial profiles of various metabolites and quantities like ATP hydrolysis rate and peak twitch force are influenced by two different structural factors—(i) total area fraction of mitochondria which determines the average concentration of phosphagens in cross sections and (ii) density distribution of mitochondria which determines the spatial distribution of phosphagens. The model also predicts nearly uniform ATP and ADP levels across the cell cross sections in normoxia due to spatial buffering by PCr and Cr. In a 3D simulation, we can similarly expect a nearly uniform ATP and ADP concentration across the cell volume irrespective of the axial distribution of mitochondrial columns. The average concentrations of the phosphagens will be determined by total volume fraction of mitochondria in the cell.

S2 Fig illustrates that different cross sections along a continuous length of the cell have similar mitochondrial area fraction as well as similar spatial variation in the mitochondrial density distribution. Since spatial distribution of metabolites like Pi, PCr and Cr depend on the distribution of mitochondria, similar mitochondrial distribution in the cross sections should also lead to similar metabolic landscapes in these cross sections. As a result, there will be negligible concentration gradient along the longitudinal axis except near areas where the myofibrils and mitochondria branch out. This also implies that a 3D simulation, which includes a 3rd dimension along the longitudinal axis of the cell, will not result in a metabolic landscape that is different from the current 2D results.

Significance of the phosphocreatine shuttle

In our model we have employed a previously postulated formulation of phosphocreatine shuttle where ATP, ADP and AMP exchange between mitochondria and myofibril is severely restricted [7, 13, 25]. As a result, more than 90% of the ATP/ADP transfer between the mitochondria and myofibril occurs via facilitated diffusion by Cr molecules instead of direct diffusion of ATP and ADP. This reliance on rapid diffusion of PCr and Cr helps the cell to maintain a uniform level of ATP and ADP in the cardiomyocytes. In the absence of the PCr and Cr facilitated diffusion, large gradients of ATP and ADP will be required to supply ATP to myofibril spaces which are far from mitochondrial clusters—thus giving rise to a non-uniform distribution of ATP and ADP. However, the cytosolic ATP pool not only acts as a source of ATP for the cross-bridge cycle, but it supports ion channel activities (e.g. SERCA pumps) and can also act as divalent metal ion chelator [40], crucial to the viability of the cell. According to a previous modelling study [41] SERCA pumps, which are intrinsic to cellular Ca²⁺ management and EC-coupling, appear to be highly sensitive to the ATP/ADP ratio in the cell. Therefore, it is vital for cardiomyocytes to maintain a uniform ATP and ADP concentration, in spite of the heterogeneous distribution of mitochondria. Our model thus suggests that phosphocreatine shuttle might be a necessary aspect of energy metabolism in cardiomyocytes with heterogeneously distributed mitochondria.

Effects of hypoxia

We used an O_2 diffusivity value (D_{O_2}) of $2.41 \times 10^{-5} \text{ cm}^2/\text{s}$ in our current simulation based on previous modelling work of Beard et al. [34]. This diffusivity value corresponds to the overall oxygen diffusion through mammalian striated muscles [42], and can be considered as an average diffusivity through all the organelles present inside a cardiomyocyte. Therefore, we did not separately model O_2 transport through the transverse tubules which are near uniformly distributed along the Z disks [43]. We also neglected the effect of myoglobin facilitated oxygen diffusion since diffusivity of myoglobin is reported to be only a small fraction ($< 1/10_{th}$) of the free O_2 diffusivity in cardiomyocytes [44]. Despite these assumptions, our model prediction of radial profiles in oxygen is consistent with previous experimental and theoretical works [29, 35]. Our model indicates that in a normoxic state, profiles of O_2 have no effect on the metabolism, and that the phosphagen distribution is dictated by the mitochondrial distribution.

However, in hypoxia, our model predicts a significant impact of O_2 profile on the phosphagen distributions and the effect of the heterogeneous mitochondrial distribution is minimal. The level of mitochondrial membrane potential in the core of the cell was substantially lower than the periphery of the cell. The ATP/ADP in the cell core was similarly depressed due to a lack of O_2 . However, these predictions are inconsistent with findings from Takahashi et al.'s 2008 work [36] exploring isolated cardiomyocytes. Takahashi et al. showed that isolated cells sustain depleted, but near homogenous levels of ATP and $\Delta\Psi$, in spite of formation of an anoxic core, when the respiration rate is elevated under a hypoxic condition. Takahashi et al. also suggested that CK mediated diffusion of PCr and Cr from the sub-sarcolemmal space supports ATP supply and $\Delta\Psi$ levels in the anoxic core for a substantial time interval before necrotic cell death. Our results contrast with this view, as they indicate that CK reaction and diffusion of PCr and Cr is not sufficient to generate a homogenous metabolic landscape under hypoxia. This inconsistency between our model predictions and experimental data suggest that other mechanisms may be at play to ensure uniform ATP supply. Other mechanisms could include glycolysis, creatine phosphate stores or $\Delta\Psi$ conductivity between sub-sarcolemmal and inter-myofibrillar mitochondria. Glancy et al recently proposed that $\Delta\Psi$ can be transmitted across the cell through mitochondrial networks in both skeletal [45] and cardiac muscle cells [11]. Transmission of $\Delta\Psi$ might be facilitated through IMJs present between adjacent mitochondria. Glancy et al. also proposed that membrane potential conduction via mitochondrial reticulæ is a dominant pathway for skeletal muscle energy distribution.

In the current study, we assumed that there is no conduction of membrane potential between adjacent mitochondria, and accordingly modelled $\Delta\Psi$ as a spatially distributed non-diffusing variable without any direct interaction between adjacent mitochondrial points. With this modelling approach, we did not find any significant difference in the mitochondrial $\Delta\Psi$ values across the cross section of the cell in normoxia. These results are consistent with Glancy et al.'s [11] observation that mitochondrial $\Delta\Psi$ conductivity is much weaker along the cell cross section compared to the longitudinal axis of the cardiomyocytes. We propose that, in normoxia, the rapid diffusion of cytosolic PCr and Cr is sufficient to maintain a uniform $\Delta\Psi$ as well as myofibrillar ATP distribution across the cell cross section without the need for $\Delta\Psi$ conduction. However, our results also imply that in a hypoxic cardiomyocyte, the phosphocreatine shuttle is not sufficient to maintain a uniform distribution of ATP. $\Delta\Psi$ conduction might play a role in maintaining uniform levels of intracellular ATP across the cell cross-section. In the future studies, it needs to be investigated whether hypoxia can lead to formation of larger number of IMJs along the cell cross section which can subsequently lead to higher $\Delta\Psi$ conductivity compared to normoxic condition.

Potential implications for diabetic cardiomyopathy

The total cellular PCr pool and activities of mitochondrial CK enzyme are severely impacted in several metabolic diseases, such as diabetic cardiomyopathy. According to previous studies [46–48], mtCK and MCK activities are suppressed by a substantial margin in diabetes (35%–50%). Without normal CK activities, homogenous ATP distribution within cardiomyocytes can be severely impacted due to heterogeneous mitochondrial distribution. Our previous studies also revealed that mitochondrial arrangement in type 1 diabetes is significantly irregular than control cells due to mitochondrial fission and clustering [9], which can also affect the distribution of cellular phosphagens. In future work, we will study these potential changes in metabolite distribution and their effect on force dynamics using a 3D geometry based FE model of cardiac bioenergetics. Future studies will also require a modification in the currently used model of mitochondrial membrane potential to incorporate the conduction of membrane potential.

Methods

Ethics statement

All animal procedures followed guidelines approved by the University of Auckland Animal Ethics Committee (for animal procedures conducted in Auckland, Application Number R826).

Tissue sample preparation and serial block face imaging

The tissue sample used for SBF-SEM imaging was collected from the left ventricular wall of a sixteen-week-old male Sprague-Dawley rat at the University of Auckland, New Zealand. We followed the guidelines approved by the University of Auckland Animal Ethics Committee (for animal procedures conducted in Auckland, Application Number R826) for the process.

Following euthanasia of the Sprague-Dawley rat, the heart was excised and quickly cannulated and connected to a Langendorff apparatus operating at a hydraulic pressure of 90 cm. We perfused the heart with a Tyrode solution including 20 mM 2,3-Butanedione Monoxime for 2–3 minutes. This was followed by perfusion with 2.5% glutaraldehyde, 2% paraformaldehyde and 50 mM CaCl₂ in 0.15 M sodium cacodylate buffer. We dissected a tissue block from the left ventricular free wall and stored in the same fixative that was precooled on ice for 2 hours. The fixative was subsequently replaced with 2% osmium tetroxide and .8% potassium ferrocyanide in 0.15 M sodium cacodylate and left overnight. Afterwards, we stained the block with ice-cold 2% uranyl acetate for 60–120 minutes. Following this, the block was washed of excess uranyl acetate and punched into a 1.5 mm diameter sample. The sample was then progressively dehydrated with ethanol followed by transition to room temperature in acetone. The sample was finally embedded in epoxy resin (Durcupan ACM resin from EM sciences).

We trimmed the tissue sample to a square block face of 1 mm² and 300 μm deep with fibers running perpendicular to the future cutting face. The sample was subsequently mounted on a Teneo VolumeScope (FEI, Hillsborough, USA) and imaged in low vacuum mode (50 mbar) with a 10 nm pixel size. We acquired a total of four thousand and nineteen serial sections of 50 nm in thickness. The sections were then aligned using IMOD. We rotated the sections by 90 degrees around the Y axis and binned the data to an isotropic voxel size of 50 x 50 x 50 nm. A detailed description of the animal procedures, sample preparation and imaging techniques is available at our previous publications [17, 18].

Model development and computational methods

As discussed earlier, the results section provides a brief description of the model development, while the supplementary document [S1 Text](#) contains description of all the PDEs, ODEs and

algebraic equation used in the model. The finite element implementation of the model was developed using reaction-diffusion module of OpenCMISS [49], an open source software package for FE simulation. Besides PDEs, the OpenCMISS model also contains ODEs and algebraic rate equations that have been described in CellML [50] models—which were solved using the Strang operator splitting method. We offer the OPECMISS implementation of the FE model for research use at https://github.com/CellSMB/cardiac_bioenergetics.

The FE models were solved on an IBM iDataplex x86 system. Individual FE models contained 300,000 FE nodes on average and required 20 hours of runtime for simulating every 1000 milliseconds of heartbeat. The results in this paper correspond to steady state solutions at 3 seconds of heartbeat time.

Supporting information

S1 Fig. Simulation of confocal microscope images from model predicted species distribution. (A) Model predicted distribution of oxygen in cross section 1 presented in grayscale image. (B) Resolution of the image predicted by the model was reduced by a margin of 5 times. (C) Subsequently, we applied a point spread function over the image, followed by application of poison noise, to derive the simulated confocal microscope image at low resolution. (PDF)

S2 Fig. Spatial variation in distribution of mitochondria and nuclei along the longitudinal axis of the cell. The black and green lines correspond to the total area fraction of mitochondria and nucleus present in each cross section of the cell. The first and third quartile of the mitochondrial density distribution in each cross section is represented using the lower and upper bound of the light blue area. There is negligible difference between the mitochondrial area fraction and quartile values of mitochondrial density distribution corresponding to different cross sections. (PDF)

S1 Text. Detailed description of the partial differential equations (PDE) based finite element model of cardiac bioenergetics. (PDF)

Acknowledgments

The authors would like to acknowledge Mr. Akter Hussain for the help with segmentation of EM images, and Melbourne Bioinformatics for the support in executing the simulations in IBM iDataplex x86 system.

Author Contributions

Conceptualization: Shouryadipta Ghosh, Edmund J. Crampin, Vijay Rajagopal.

Data curation: Vijay Rajagopal.

Formal analysis: Shouryadipta Ghosh, Anthony J. R. Hickey, Vijay Rajagopal.

Funding acquisition: Edmund J. Crampin, Vijay Rajagopal.

Investigation: Shouryadipta Ghosh, Kenneth Tran, Anthony J. R. Hickey, Vijay Rajagopal.

Methodology: Shouryadipta Ghosh, Kenneth Tran, Vijay Rajagopal.

Project administration: Vijay Rajagopal.

Resources: Anthony J. R. Hickey, Eric Hanssen.

Software: Shouryadipta Ghosh, Kenneth Tran, Vijay Rajagopal.

Supervision: Lea M. D. Delbridge, Eric Hanssen, Edmund J. Crampin, Vijay Rajagopal.

Validation: Shouryadipta Ghosh, Kenneth Tran, Vijay Rajagopal.

Visualization: Shouryadipta Ghosh, Eric Hanssen, Vijay Rajagopal.

Writing – original draft: Shouryadipta Ghosh, Kenneth Tran.

Writing – review & editing: Shouryadipta Ghosh, Kenneth Tran, Lea M. D. Delbridge, Anthony J. R. Hickey, Eric Hanssen, Edmund J. Crampin, Vijay Rajagopal.

References

1. Bittl JA, Ingwall JS. Reaction rates of creatine kinase and ATP synthesis in the isolated rat heart. A 31P NMR magnetization transfer study. *Journal of Biological Chemistry*. 1985; 260(6):3512–7. PMID: [3972835](#)
2. Katz LA, Swain JA, Portman MA, Balaban RS. Relation between phosphate metabolites and oxygen consumption of heart in vivo. *American Journal of Physiology-Heart and Circulatory Physiology*. 1989; 256(1):H265–H74. <https://doi.org/10.1152/ajpheart.1989.256.1.H265> PMID: [2912189](#).
3. Williamson JR, Ford C, Illingworth J, Safer B. Coordination of citric acid cycle activity with electron transport flux. *Circulation research*. 1976; 38(5 Suppl 1):I39–I51.
4. Vendelin M, Béraud N, Guerrero K, Andrienko T, Kuznetsov AV, Olivares J, et al. Mitochondrial regular arrangement in muscle cells: a “crystal-like” pattern. *American Journal of Physiology—Cell Physiology*. 2005; 288(3):C757–C67. <https://doi.org/10.1152/ajpcell.00281.2004> PMID: [15496480](#)
5. Birkedal R, Shiels HA, Vendelin M. Three-dimensional mitochondrial arrangement in ventricular myocytes: from chaos to order. *American Journal of Physiology—Cell Physiology*. 2006; 291(6):C1148–C58. <https://doi.org/10.1152/ajpcell.00236.2006> PMID: [16822946](#)
6. Vendelin M, Eimre M, Seppet E, Peet N, Andrienko T, Lemba M, et al. Intracellular diffusion of adenosine phosphates is locally restricted in cardiac muscle. *Molecular and cellular biochemistry*. 2004; 256-257(1–2):229–41. Epub 2004/02/24. PMID: [14977184](#).
7. Seppet EK, Eimre M, Anmann T, Seppet E, Peet N, Käambre T, et al. Intracellular energetic units in healthy and diseased hearts. *Experimental & Clinical Cardiology*. 2005; 10(3):173–83. PubMed PMID: [PMC2716248](#).
8. Seppet EK, Eimre M, Anmann T, Seppet E, Piirsoo A, Peet N, et al. Structure-function relationships in the regulation of energy transfer between mitochondria and ATPases in cardiac cells. *Experimental & Clinical Cardiology*. 2006; 11(3):189–94. PubMed PMID: [PMC2276156](#).
9. Jarosz J, Ghosh S, Delbridge LMD, Petzer A, Hickey AJR, Crampin EJ, et al. Changes in mitochondrial morphology and organization can enhance energy supply from mitochondrial oxidative phosphorylation in diabetic cardiomyopathy. *American Journal of Physiology—Cell Physiology*. 2017; 312(2):C190–C7. <https://doi.org/10.1152/ajpcell.00298.2016> PMID: [27903587](#)
10. Lavorato M, Iyer VR, Dewight W, Cupo RR, Debattisti V, Gomez L, et al. Increased mitochondrial nano-tunneling activity, induced by calcium imbalance, affects intermitochondrial matrix exchanges. *Proceedings of the National Academy of Sciences*. 2017; 114(5):E849–E58. <https://doi.org/10.1073/pnas.1617788113> PMID: [28096415](#)
11. Glancy B, Hartnell LM, Combs CA, Fenmou A, Sun J, Murphy E, et al. Power Grid Protection of the Muscle Mitochondrial Reticulum. *Cell Reports*. 2017; 19(3):487–96. <https://doi.org/10.1016/j.celrep.2017.03.063> PMID: [28423313](#)
12. Tsushima K, Bugger H, Wende AR, Soto J, Jenson GA, Tor AR, et al. Mitochondrial Reactive Oxygen Species in Lipotoxic Hearts Induces Post-Translational Modifications of AKAP121, DRP1 and OPA1 That Promote Mitochondrial Fission. *Circulation Research*. 2017. <https://doi.org/10.1161/circresaha.117.311307> PMID: [29092894](#)
13. Vendelin M, Kongas O, Saks V. Regulation of mitochondrial respiration in heart cells analyzed by reaction-diffusion model of energy transfer. *American Journal of Physiology—Cell Physiology*. 2000; 278(4):C747–C64. <https://doi.org/10.1152/ajpcell.2000.278.4.C747> PMID: [10751324](#)
14. Hatano A, Okada J-i, Washio T, Hisada T, Sugiura S. A Three-Dimensional Simulation Model of Cardiomyocyte Integrating Excitation-Contraction Coupling and Metabolism. *Biophysical Journal*. 2011; 101(11):2601–10. <https://doi.org/10.1016/j.bpj.2011.10.020> PMID: [22261047](#)
15. Hatano A, Okada J-i, Washio T, Hisada T, Sugiura S. Mitochondrial Colocalization with Ca²⁺ Release Sites is Crucial to Cardiac Metabolism. *Biophysical Journal*. 2013; 104(2):496–504. <https://doi.org/10.1016/j.bpj.2012.12.004> PMID: [23442872](#)

16. Hatano A, Okada J-i, Washio T, Hisada T, Sugiura S. Distinct Functional Roles of Cardiac Mitochondrial Subpopulations Revealed by a 3D Simulation Model. *Biophysical Journal*. 2015; 108(11):2732–9. <https://doi.org/10.1016/j.bpj.2015.04.031>. PMID: 26039174
17. Hussain A, Hanssen E, Rajagopal V. A Semi-Automated Workflow for Segmenting Contents of Single Cardiac Cells from Serial-Block-Face Scanning Electron Microscopy Data. *Microscopy and Microanalysis*. 2017; 23(S1):240–1. Epub 2017/08/04. <https://doi.org/10.1017/S143192761700188X>
18. Hussain A, Ghosh S, Kalkhoran SB, Hausenloy DJ, Hanssen E, Rajagopal V. An automated workflow for segmenting single adult cardiac cells from large-volume serial block-face scanning electron microscopy data. *Journal of Structural Biology*. 2018. <https://doi.org/10.1016/j.jsb.2018.02.005>.
19. Kremer JR, Mastrorade DN, McIntosh JR. Computer Visualization of Three-Dimensional Image Data Using IMOD. *Journal of Structural Biology*. 1996; 116(1):71–6. <https://doi.org/10.1006/jsbi.1996.0013>. PMID: 8742726
20. Rajagopal V, Bass G, Ghosh S, Hunt H, Walker C, Hanssen E, et al. Creating a Structurally Realistic Finite Element Geometric Model of a Cardiomyocyte to Study the Role of Cellular Architecture in Cardiomyocyte Systems Biology. *JoVE*. 2018;(134):e56817. <https://doi.org/10.3791/56817> PMID: 29733314
21. Picard M, McManus MJ, Csordás G, Várnai P, Dorn GW II, Williams D, et al. Trans-mitochondrial coordination of cristae at regulated membrane junctions. *Nature communications*. 2015; 6.
22. Beard DA. A Biophysical Model of the Mitochondrial Respiratory System and Oxidative Phosphorylation. *PLoS Comput Biol*. 2005; 1(4):e36. <https://doi.org/10.1371/journal.pcbi.0010036> PMID: 16163394
23. Wu F, Zhang EY, Zhang J, Bache RJ, Beard DA. Phosphate metabolite concentrations and ATP hydrolysis potential in normal and ischaemic hearts. *The Journal of physiology*. 2008; 586(17):4193–208. <https://doi.org/10.1113/jphysiol.2008.154732> PMID: 18617566
24. Aliev MK, Saks VA. Compartmentalized energy transfer in cardiomyocytes: use of mathematical modeling for analysis of in vivo regulation of respiration. *Biophysical Journal*. 1997; 73(1):428–45. [https://doi.org/10.1016/S0006-3495\(97\)78082-2](https://doi.org/10.1016/S0006-3495(97)78082-2). PMID: 9199806
25. Simson P, Jephthina N, Laasmaa M, Peterson P, Birkedal R, Vendelin M. Restricted ADP movement in cardiomyocytes: Cytosolic diffusion obstacles are complemented with a small number of open mitochondrial voltage-dependent anion channels. *Journal of Molecular and Cellular Cardiology*. 2016; 97:197–203. <https://doi.org/10.1016/j.yjmcc.2016.04.012>. PMID: 27261153
26. Dieteren CEJ, Gielen SCAM, Nijtmans LGJ, Smeitink JAM, Swarts HG, Brock R, et al. Solute diffusion is hindered in the mitochondrial matrix. *Proceedings of the National Academy of Sciences*. 2011; 108(21):8657–62. <https://doi.org/10.1073/pnas.1017581108> PMID: 21555543
27. Tran K, Smith NP, Loisel DS, Crampin EJ. A metabolite-sensitive, thermodynamically constrained model of cardiac cross-bridge cycling: implications for force development during ischemia. *Biophysical journal*. 2010; 98(2):267–76. <https://doi.org/10.1016/j.bpj.2009.10.011> PMID: 20338848
28. Saks VA, Ventura-Clapier R, (Editors). *Cellular Bioenergetics: Role of Coupled Creatine Kinases*. Boston, MA: Kluwer Academic; 1994. 346 p.
29. Takahashi E, Sato K, Endoh H, Xu Z-L, Doi K. Direct observation of radial intracellular P_o2 gradients in a single cardiomyocyte of the rat. *American Journal of Physiology-Heart and Circulatory Physiology*. 1998; 275(1):H225–H33.
30. Rajagopal V, Bass G, Walker CG, Crossman DJ, Petzer A, Hickey A, et al. Examination of the Effects of Heterogeneous Organization of RyR Clusters, Myofibrils and Mitochondria on Ca²⁺ Release Patterns in Cardiomyocytes. *PLoS Comput Biol*. 2015; 11(9):e1004417. <https://doi.org/10.1371/journal.pcbi.1004417> PMID: 26335304
31. Mik EG, Ince C, Eerbeek O, Heinen A, Stap J, Hooibrink B, et al. Mitochondrial oxygen tension within the heart. *Journal of Molecular and Cellular Cardiology*. 2009; 46(6):943–51. <https://doi.org/10.1016/j.yjmcc.2009.02.002>. PMID: 19232352
32. Kennedy FG, Jones DP. Oxygen dependence of mitochondrial function in isolated rat cardiac myocytes. *American Journal of Physiology-Cell Physiology*. 1986; 250(3):C374–C83. <https://doi.org/10.1152/ajpcell.1986.250.3.C374> PMID: 3953808.
33. Rumsey WL, Schlosser C, Nuutinen EM, Robiolio M, Wilson DF. Cellular energetics and the oxygen dependence of respiration in cardiac myocytes isolated from adult rat. *Journal of Biological Chemistry*. 1990; 265(26):15392–402. PMID: 2394731
34. Beard DA, Bassingthwaite JB. Modeling Advection and Diffusion of Oxygen in Complex Vascular Networks. *Ann Biomed Eng*. 2001; 29(4):298–310. <https://doi.org/10.1114/1.1359450> PMID: 11339327
35. Groebe K. An easy-to-use model for O₂ supply to red muscle. Validity of assumptions, sensitivity to errors in data. *Biophysical Journal*. 1995; 68(4):1246–69. [https://doi.org/10.1016/S0006-3495\(95\)80300-0](https://doi.org/10.1016/S0006-3495(95)80300-0) PMID: 7787016

36. Takahashi E. Anoxic cell core can promote necrotic cell death in cardiomyocytes at physiological extracellular Po₂. *American Journal of Physiology-Heart and Circulatory Physiology*. 2008; 294(6):H2507–H15. <https://doi.org/10.1152/ajpheart.00168.2008> PMID: 18424639.
37. Ebus JP, Papp Z, Zaremba R, Stienen GJ. Effects of MgATP on ATP utilization and force under normal and simulated ischaemic conditions in rat cardiac trabeculae. *Pflügers Archiv: European Journal Of Physiology*. 2001; 443(1):102–11. <https://doi.org/10.1007/s004240100667> PMID: 11692273.
38. Fukuda N, Fujita H, Fujita T, Ishiwata Si. Regulatory roles of MgADP and calcium in tension development of skinned cardiac muscle. *Journal of Muscle Research and Cell Motility*. 1998; 19(8):909–21. <https://doi.org/10.1023/A:1005437517287>. PMID: 10047990; 763581226.
39. Tewari SG, Bugenhagen SM, Palmer BM, Beard DA. Dynamics of cross-bridge cycling, ATP hydrolysis, force generation, and deformation in cardiac muscle. *Journal of Molecular and Cellular Cardiology*. 2016; 96:11–25. <https://doi.org/10.1016/j.yjmcc.2015.02.006>. PMID: 25681584
40. Morcos NC, Jacobson AL. Calcium binding in cardiac sarcolemma. *Canadian Journal of Physiology and Pharmacology*. 1979; 57(5):529–34. <https://doi.org/10.1139/y79-080> PMID: 157217
41. Tran K, Smith NP, Loiselle DS, Crampin EJ. A thermodynamic model of the cardiac sarcoplasmic/endoplasmic Ca²⁺(SERCA) pump. *Biophysical journal*. 2009; 96(5):2029–42. <https://doi.org/10.1016/j.bpj.2008.11.045> PMID: 19254563
42. Bentley TB, Meng H, Pittman RN. Temperature dependence of oxygen diffusion and consumption in mammalian striated muscle. *American Journal of Physiology-Heart and Circulatory Physiology*. 1993; 264(6):H1825–H30. <https://doi.org/10.1152/ajpheart.1993.264.6.H1825> PMID: 8322911.
43. Brette F, Orchard C. T-Tubule Function in Mammalian Cardiac Myocytes. *Circulation Research*. 2003; 92(11):1182–92. <https://doi.org/10.1161/01.RES.0000074908.17214.FD> PMID: 12805236
44. Papadopoulos S, Endeward V, Revesz-Walker B, Jürgens KD, Gros G. Radial and longitudinal diffusion of myoglobin in single living heart and skeletal muscle cells. *Proceedings of the National Academy of Sciences*. 2001; 98(10):5904–9. <https://doi.org/10.1073/pnas.101109798> PMID: 11320218
45. Glancy B, Hartnell LM, Malide D, Yu Z-X, Combs CA, Connelly PS, et al. Mitochondrial reticulum for cellular energy distribution in muscle. *Nature*. 2015; 523(7562):617–20. <https://doi.org/10.1038/nature14614> <http://www.nature.com/nature/journal/v523/n7562/abs/nature14614.html#supplementary-information>. PMID: 26223627
46. Savabi F, Kirsch A. Alteration of the phosphocreatine energy shuttle components in diabetic rat heart. *Journal of Molecular and Cellular Cardiology*. 1991; 23(11):1323–33. [https://doi.org/10.1016/0022-2828\(91\)90089-5](https://doi.org/10.1016/0022-2828(91)90089-5). PMID: 1803023
47. Spindler M, Saupe KW, Tian R, Ahmed S, Matlib MA, Ingwall JS. Altered Creatine Kinase Enzyme Kinetics in Diabetic Cardiomyopathy. A31P NMR Magnetization Transfer Study of the Intact Beating Rat Heart. *Journal of Molecular and Cellular Cardiology*. 1999; 31(12):2175–89. <https://doi.org/10.1006/jmcc.1999.1044>. PMID: 10640445
48. Popovich BK, Boheler KR, Dillmann WH. Diabetes decreases creatine kinase enzyme activity and mRNA level in the rat heart. *American Journal of Physiology-Endocrinology and Metabolism*. 1989; 257(4):E573–E7. <https://doi.org/10.1152/ajpendo.1989.257.4.E573> PMID: 2679131.
49. Bradley C, Bowery A, Britten R, Budelmann V, Camara O, Christie R, et al. OpenCMISS: a multi-physics & multi-scale computational infrastructure for the VPH/Physiome project. *Progress in biophysics and molecular biology*. 2011; 107(1):32–47. <https://doi.org/10.1016/j.pbiomolbio.2011.06.015> PMID: 21762717
50. Garry A, Nickerson D, Cooper J, Santos R, Miller A, McKeever S, et al. CellML and associated tools and techniques. *Philosophical Transactions A*. 2008; 366. <https://doi.org/10.1098/rsta.2008.0094> PMID: 18579471